CFD Simulations of the IHF 13-Inch Nozzle Flow: 55-deg Sphere-Cone Model, Manufactured Fences and Gaps

Tahir Gökçen,¹ Tane Boghozian,² and Antonella I. Alunni³ *AMA Inc.*, *NASA Ames Research Center, Moffett Field, CA 94035*

This paper reports computational analyses of tests in a high enthalpy arc-jet facility at NASA Ames Research Center. These tests were conducted using 55-deg sphere-cone models placed in a free jet downstream of the 13-inch diameter conical nozzle in the Ames 60-MW Interaction Heating Facility. Some of the sphere-cone models include surface features such as manufactured fences and gaps intended to simulate effects of differential recession, all of which disturb the flow, producing augmented heating locally and downstream. Test calibration data were obtained using slug and Gardon gage stagnation calorimeters, and a sphere-cone calorimeter model with six Gardon gages and five pressure tabs. The present analysis comprises computational fluid dynamics simulations of the nonequilibrium flowfield in the facility nozzle and test box, including the models tested, and comparisons with the experimental measurements. These simulations take into account nonuniform total enthalpy and mass flux profiles at the nozzle inlet as well as the expansion waves emanating from the nozzle exit and their effects on the model flowfields.

I. Nomenclature

```
= species mass fraction for species i
C_i
D_e
          = nozzle exit diameter, cm (or in)
              enthalpy, MJ/kg
          = total enthalpy, MJ/kg
h_o
          = mass-averaged total enthalpy (or bulk enthalpy), MJ/kg
          = centerline total enthalpy, MJ/kg
h_{ocl}
Ι
          = arc current, A
M
          = Mach number
              Mach number at the boundary layer edge
M_{o}
              total mass flow rate, g/s
m
              arc heater main air flow rate, g/s
              add-air flow rate or cold-gas injection rate at the plenum, g/s
\dot{m}_a
          = argon flow rate, g/s
\dot{m}_{ar}
              pressure, kPa
p
          = test box pressure, torr
p_{box}
              arc-heater pressure, kPa
p_{ch}
          = total pressure, kPa
p_o
              surface pressure, kPa
p_s
              pitot pressure or model stagnation pressure, kPa
              pressure gages on the sphere-cone calorimeter (Fig. 2a)
p_1 - p_5
              heat flux gages on the sphere-cone calorimeter (Fig. 2a)
Q_1–Q_6
              cold-wall full-catalytic heat flux, W/cm<sup>2</sup>
q_{CWFC}
          = hot-wall full-catalytic heat flux (radiative equilibrium), W/cm<sup>2</sup>
QHWFC
          = surface heat flux, W/cm<sup>2</sup>
          = model corner radius, m
```

¹ Senior Research Scientist, MS 230-2, Associate Fellow AIAA

² Material Scientist, MS 234-1

_

³ Research Scientist, MS 229-1 (currently Aerospace Engineer, Entry Systems and Vehicle Development Branch)

 r_n = nose radius, m

s = arc-length coordinate from stagnation point, m

T = temperature or translational-rotational temperature, K

 T_{ν} = vibrational-electronic temperature, K

 T_s = surface temperature, K

V = arc voltage, V

 x_{ml} = model location from the nozzle exit plane, cm

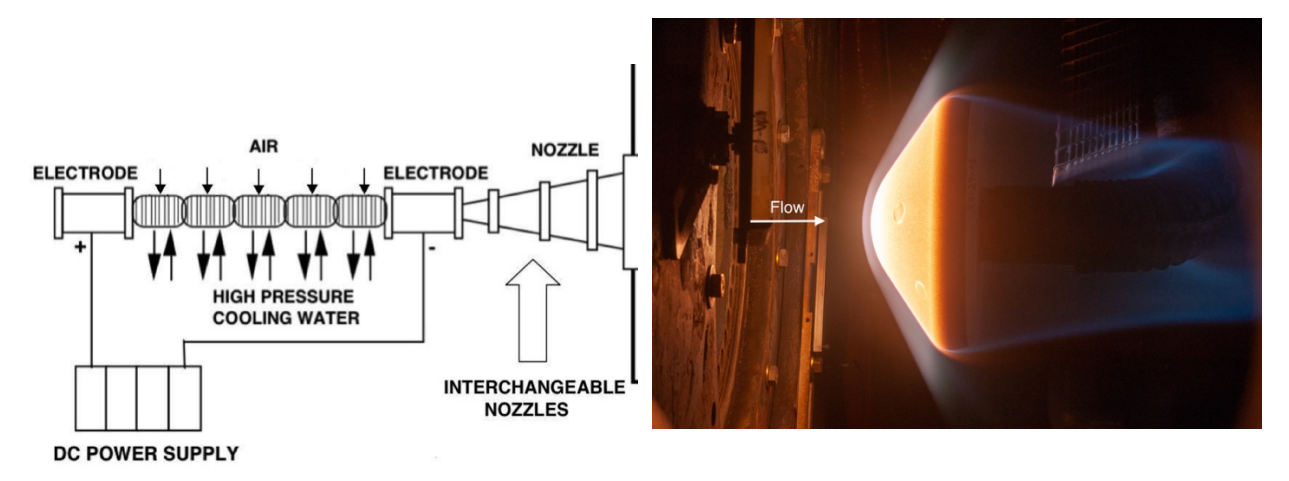
 δ = boundary layer thickness, cm

 τ_s = surface shear, Pa

II. Introduction

Arc-jet facilities provide the primary means to study the performance of various types of thermal protection systems (TPS) used on the outer surfaces of spacecraft in an aerothermodynamic heating environment. In a high enthalpy arc-jet facility, a test gas, usually air or a mixture of nitrogen, oxygen and argon, is passed through an electric arc discharge where the energy is added to the flow. The test gas is then expanded through a converging-diverging nozzle into an evacuated test chamber to produce high-enthalpy supersonic or hypersonic flow. NASA Ames Research Center (ARC) has four arc-jet facilities within its Arc-Jet Complex [1]. Among the various arc-jet test configurations, the two most frequently used are in conical and semi-elliptical nozzles. In the conical nozzle test configurations, stagnation pucks or wedge models are placed in a free jet downstream of the nozzle. In the semi-elliptical nozzle configuration, test articles, which are usually flat panels, are mounted flush to the bottom surface of the nozzle in a supersonic jet at the nozzle exit. For the present tests, one of the arc-jet facilities at NASA ARC, the Interaction Heating Facility (IHF) has been used to test relatively large, 23.6-cm diameter, 55-deg sphere-cone models in the conical nozzle test configuration. Although the sphere-cone model is similar to stagnation pucks, due to its relatively large size, it enables testing TPS materials in combinations of heat flux, pressure and shear different from those accessible in the various wedge tests (e.g., see [2-5]). Also, some of the sphere-cone models include surface features such as manufactured fences and gaps. These surface features are intended to simulate the effects of differential recession that could be present in flight. The fences and gaps disturb the flow, producing augmented heating locally and downstream.

In support of these tests, computational fluid dynamics (CFD) simulations are used to characterize the arc-jet test environment and its parameters consistent with the facility and calibration measurements and to provide surface quantities and input for material thermal response analyses. The primary objective of the paper is to report these CFD simulations. The present analysis comprises computational Navier-Stokes simulations of the nonequilibrium flowfield in the facility nozzle and test box as well as the flowfield over the models, and comparisons with the calibration data.



(a) IHF arc-heater/nozzles sketch

(b) 55-deg sphere-cone model test

Figure 1. IHF sketch and a photograph of IHF 13-inch nozzle test.

III. Arc-Jet Facility and Tests

The Interaction Heating Facility (IHF) at NASA ARC consists of a constricted arc heater, a 60-MW DC power supply, interchangeable conical and semi-elliptical nozzles, a test chamber, and supplementary systems including steam ejector vacuum system, cooling-water system and data acquisition system. The IHF is designed to operate with a set of conical nozzles or a semi-elliptical nozzle at total pressures of 1-9 atm and total bulk enthalpies of 2-28 MJ/kg (air) [6]. The 60-MW constricted arc heater produces high-temperature test gas for both nozzle configurations. The conical nozzle configurations of the IHF are suitable for tests of stagnation coupon and blunted wedge models in hypersonic flow, while the semi-elliptical nozzle configuration is designed mainly for testing flat panels in hypersonic boundary-layer heating environments. Figure 1 shows a schematic diagram of the IHF with its interchangeable nozzles and a photograph of a 55-deg sphere-cone test in the IHF 13-inch nozzle.

The IHF 13-inch conical nozzle, like the other IHF conical nozzles, has a throat diameter of 6.033 cm (2.375 in) and 10° half-angle for the diverging section, and it has an exit diameter of 33.02 cm (13 in). The 26.3-cm diameter sphere-cone model has a 55° half-angle, a nose radius of 7.62 cm (3 in), and 2.03 cm (0.8 in) corner radius. The model size is close to the maximum size that can be tested in the 13-inch nozzle without flow spillage over the diffuser and related flow quality concerns.





(a) 26.3-cm 55° sphere-cone Gardon gage calorimeter





(b) 10.2-cm iso-q slug calorimeter

(c) 10.2-cm iso-q Gardon gage calorimeter

Figure 2. Photographs of the calorimeter models used to calibrate arc-jet test conditions.

For the present paper, while analyses of the 55° sphere-cone conducted using the IHF 13-inch nozzle, designated as IHF 352 test series, are of primary interest, analyses of calibration tests performed earlier at similar conditions (IHF 345 tests) will also be considered.

Figure 2 shows photographs of the calorimeter models used to calibrate arc-jet test conditions. Both slug and Gardon gage calorimeters for heat flux measurements [7, 8] are used. The 55° sphere-cone Gardon gage calorimeter model has the same shape as the smooth surface test articles, and it is water cooled and instrumented with 6 Gardon

gage heat flux sensors and 5 pressure transducers. The other two colorimeters, 10.2-cm diameter slug and Gardon gage calorimeters, are iso-q (constant heat flux) shape. The so-called iso-q model shape consists of a spherical segment nosecap, with nose radius equal to the model diameter. The shoulder region of the nosecap is rounded to the cylindrical sides $(r_c/r_n = 1/16)$.

Note that in IHF 352 test series, four different types of test articles with the same 55° sphere-cone shape were instrumented with five thermocouple plugs and tested: one smooth surface (control), one with flush seams, one with manufactured fences, and one with manufactured gaps. The sphere-cone models were tested at three arc-jet conditions. Summaries of facility conditions and stagnation calorimeter data for the three conditions of IHF 352 tests are listed in Table 1. Note that Table 1 includes only 10.2-cm iso-q slug calorimeter data. All of the Gardon gage data will also be included in the proposed paper.

Table 1. Summary of facility conditions and stagnation slug calorimeter data obtained in the IHF 13-inch nozzle at $x_{ml} = 15.24$ cm, IHF 352 tests.

	IHF 352 Tests Facility/Calibration Data		
p _{ch} , kPa	Cond 1 805	Cond 2 346	Cond 3 254
I, A	5996	3492	2195
V, V	6592	3848	3345
ṁ, g∕s	849	451	377
\dot{m}_m	740	240	170
\dot{m}_a	55	180	180
\dot{m}_{ar}	54	31	27
$h_{ob}(W)$, MJ/kg	20.1	11.8	8.5
qisoq, W/cm ²	627	267	169
pisoq, kPa	37.3	15.9	11.5

The facility bulk enthalpy estimates, $h_{ob}(W)$, are determined by the equilibrium sonic flow method of Winovich [9].

Cond 1: Runs 2-1, 4-1, 5-1, 6-1, and 14-1

Cond 2: Runs 1-2, 2-2, 7-2, 8-2, 9-2, 10-2, 14-2, and 15-2

Cond 3: Runs 1-3, 3-3, 11-3, 12-3, 13-3, and 15-3

IV. Computational Approach

Computational analyses of arc-jet tests are performed through simulation of nonequilibrium expanding flow in the arc-jet nozzle and supersonic jet, and simulation of the flow in the test box and around the test articles. For all CFD calculations, the Data Parallel Line Relaxation (DPLR) code [10, 11], a NASA Ames in-house flow solver, is used. DPLR has been employed extensively at Ames for hypersonic flight, planetary entry and arc-jet simulations. DPLR provides various options for thermophysical models and formulation. For CFD calculations presented in this paper, two-dimensional axisymmetric or three-dimensional Navier-Stokes equations, supplemented with the equations accounting for nonequilibrium kinetic processes, are used in the formulation. The thermochemical model employed for the arc-jet flow includes six species (N₂ O₂, NO, N, O, Ar), and the thermal state of the gas is described by two temperatures (translational-rotational and vibrational-electronic) within the framework of Park's two-temperature model [12].

The flowfield in an arc-jet facility, from the arc heater to the test section, is a very complex, three-dimensional flow with various nonequilibrium processes occurring. In order to simulate the flowfield, several simplifying assumptions are made, and corresponding numerical boundary conditions are prescribed for CFD simulations. The present computational approach follows our earlier work [13, 14, 5], and it is also briefly described here. Simulations

of the arc-jet facility flow are started from the nozzle inlet. The total enthalpy and its radial profile at the inlet are prescribed based on the facility and calibration data, and the flow properties at the inlet are assumed to be in thermochemical equilibrium. Measured facility data, namely, the total pressure, mass flow rate, and test box pressure, are used as boundary conditions. The calibration data obtained include stagnation calorimeter heat flux and pressure in the freestream, and pressure and heat flux measurements on the 55-deg sphere-cone calorimeter. All metallic surfaces, water-cooled nozzle walls, and calorimeter model surfaces (copper slug or Gardon gages), are assumed to be fully catalytic to recombination reactions of atomic oxygen and nitrogen at a constant temperature of 500 K. The test box is included in the CFD simulations, primarily to account for the free jet expansion formed by the under-expanded flow exiting the nozzle to the test box and its potential effects on model flowfields. The jet expansion within the test box is primarily determined by the test box static pressure, which is one of the facility measurements and is prescribed as a boundary condition.

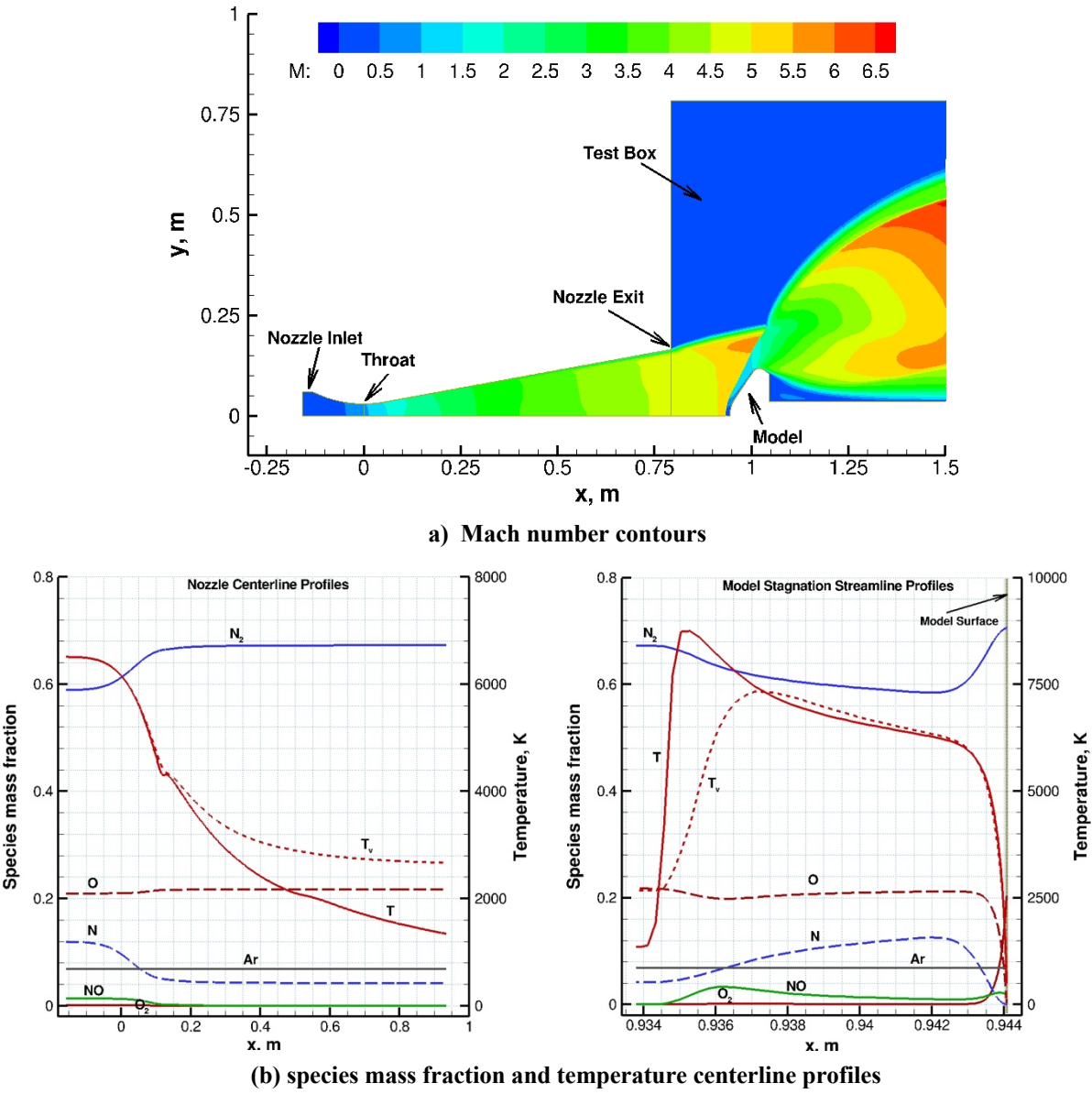


Figure 3. Computed IHF 13-inch nozzle flowfield including the test box and smooth sphere-cone model: $\dot{m} = 451 \text{ g/s}$, $h_{ob} = 13.1 \text{ MJ/kg}$, $h_{ocl} = 15.4 \text{ MJ/kg}$, parabolic profile, air with 6.9% Ar, $p_{box} = 2 \text{ torr}$.

V. Computational Results

As an illustration of a typical axisymmetric simulation, Fig. 3 shows a computed IHF 13-inch nozzle flowfield including the test box and 55-deg sphere-cone model. The extent of flow expansion at the nozzle exit (for the jet exiting to the test box) and its interactions with the model shock wave is primarily determined by the test box pressure. In Fig. 3a, computed Mach number contours are shown. The expansion waves emanating from the nozzle lip at the exit to the test box and their interaction with the bow shock wave of the model are clearly seen. These affect the shape and strength of the shock wave, thus affecting the flowfield downstream. In order to provide some insight into the nonequilibrium flowfield chemistry within the nozzle, species mass fraction and temperature profiles are shown in Fig. 3b. Because of the nonequilibrium expansion process in the nozzle, the chemical composition freezes near the throat where the flow is dissociated and vibrationally excited. As shown in Fig. 3b, for this case, at this pressure and moderately high enthalpy level, the computations predict that the flow is chemically frozen but remains in vibrational nonequilibrium before it reaches the nozzle exit. Note that oxygen remains fully dissociated within the entire flowfield except in the boundary layer near the walls, while nitrogen is partially dissociated.

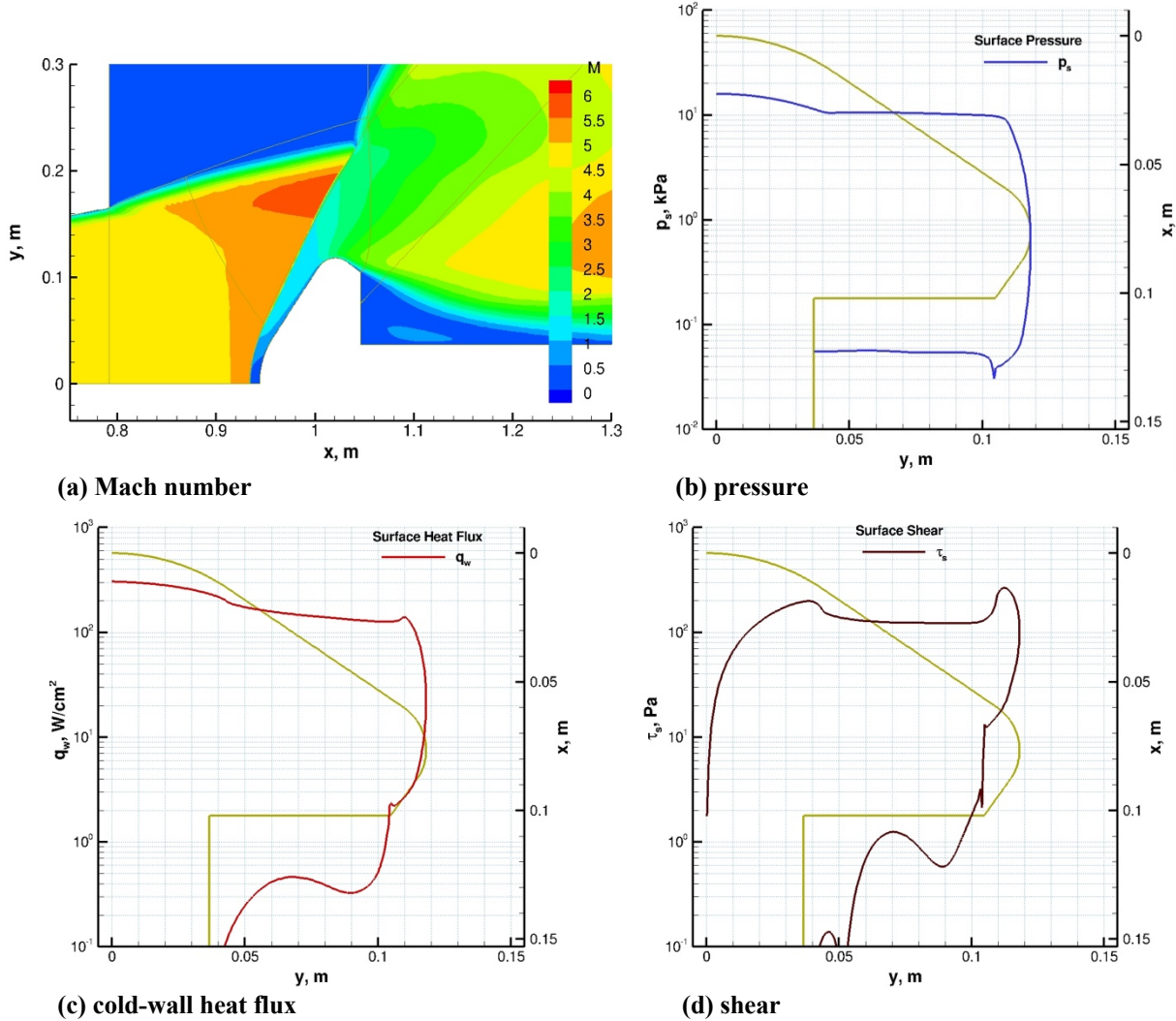


Figure 4. Computed flowfield and sphere-cone model surface quantities. IHF 13-inch nozzle flow (IHF 352, cond 2): $\dot{m} = 451$ g/s, $h_{ob} = 13.1$ MJ/kg, $h_{ocl} = 15.4$ MJ/kg, parabolic profile, air with 6.9% Ar, $p_{box} = 2$ torr.

Figure 4 shows computed flowfield and model surface quantities for IHF 352 condition 2. Figure 4a shows the computed Mach number contours around the test article. The centerline total enthalpy of the arc-jet flow is inferred from 10.2-cm diameter iso-q slug calorimeter measurements and CFD simulations. The estimation of centerline total

enthalpy from the calorimeter measurements this way (e.g., see Refs. [3-5]) is analogous to the ASTM standard E637-05 [15], except that the heat transfer theory used in the standard is replaced by CFD simulations.

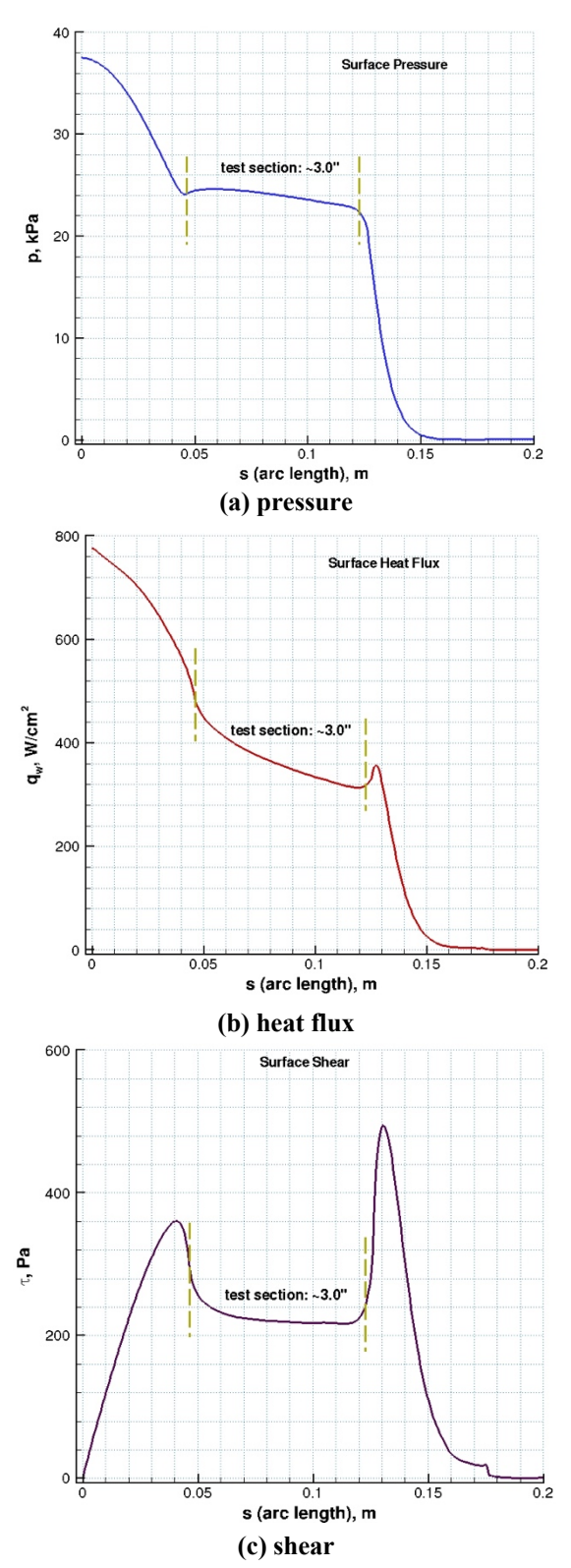


Figure 5. Computed sphere-cone model surface quantities (forebody). IHF 13-inch nozzle flow (IHF 345, cond 1): $\dot{m} = 849$ g/s, $h_{ob} = 22.3$ MJ/kg, $h_{ocl} = 23.7$ MJ/kg, parabolic profile, air with 6.4% Ar, $p_{box} = 4$ torr.

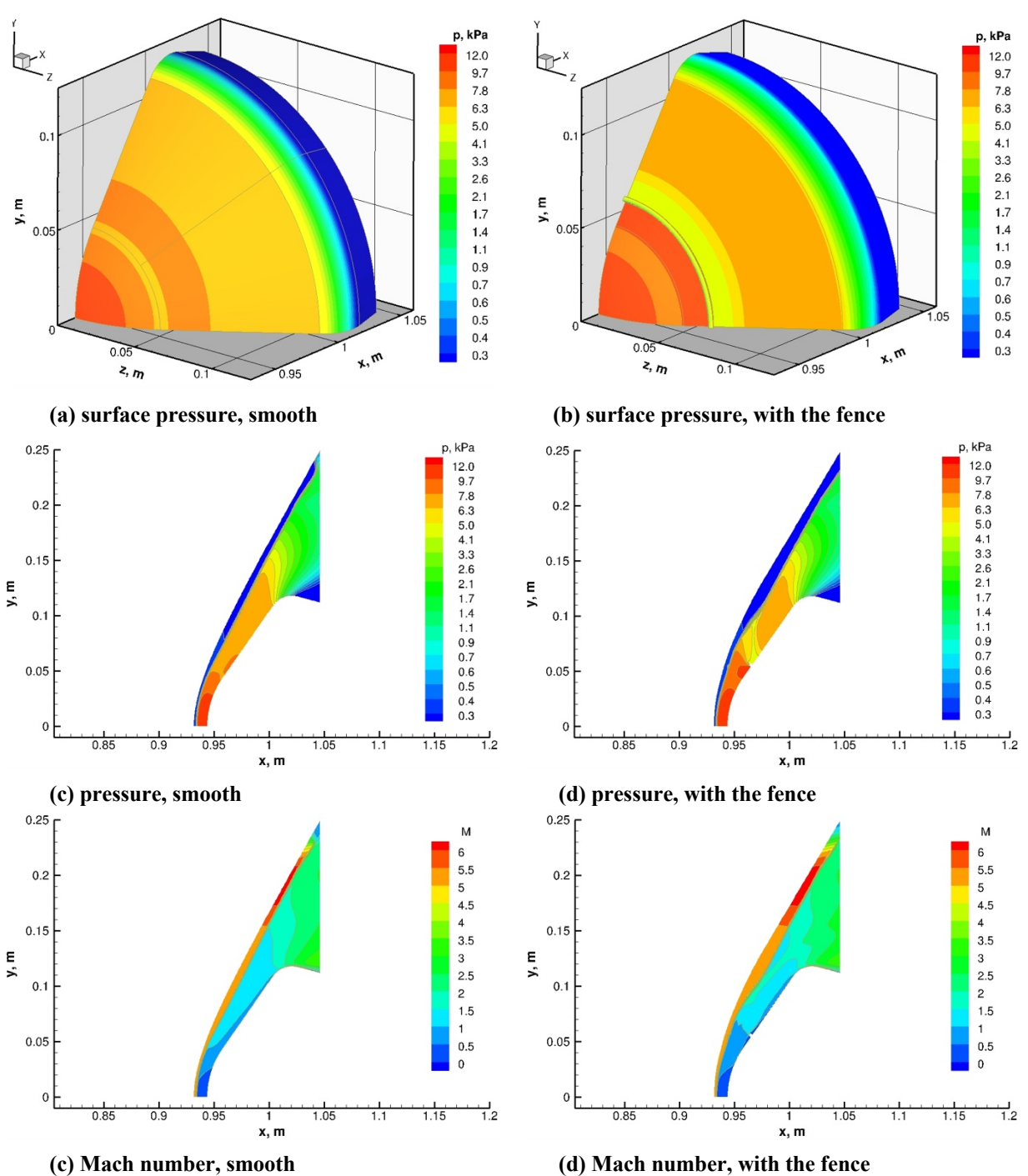


Figure 6. Computed model surface pressures and xy-symmetry flowfield contours for the two models (smooth and with a 2.5 mm fence). IHF 13-inch nozzle flow: $\dot{m} = 377$ g/s, $h_{ob} = 9.6$ MJ/kg, $h_{ocl} = 12.0$ MJ/kg, parabolic profile, air with 7.2% Ar, $p_{box} = 1$ torr.

Note that the computed surface quantities on the conical flank section of the model are relatively uniform, especially surface pressure and shear. Because of that, the conical flank section (test section of the model) is considered ideal for obtaining thermal material response data, and the models were instrumented with thermocouple plugs distributed on the flank section as well as at the stagnation point.

Figure 5 shows computed surface quantities of the smooth sphere-cone model forebody at IHF 345 condition 1. This condition is close to the facility maximum in terms of arc heater current and mass flow rate, so the surface quantities (heat flux, pressure and shear) are also close to the maximum achievable in this test configuration.

As preliminary simulation results, Fig. 6 shows computed surface pressure contours, and xy-symmetry plane flowfield contours for a smooth model and a model with a 2.5 mm manufactured fence. Clearly, the presence of a fence on the model surface disturbs the flow including the bow shock wave, thus affecting distributions of all surface quantities. Although details of the flowfield near the fence region are not shown here, complex flow structures exist at both upstream and downstream of the fence. A primary separation bubble is formed at the leading edge of the fence, which interacts with oncoming subsonic boundary layer. As the flow expands over the fence, another separated region is formed right behind the fence. When the flow downstream finally reattaches, it is manifested in augmented heating.

Analyses of the test data obtained are currently in progress. In the proposed paper, further details of the computed flowfields for the sphere-cone models and comparisons with the calibration and test data will be presented.

Acknowledgments

This work was funded by the NASA Orion TPS Insight/Oversight project. The arc-jet operational capability at NASA ARC is also supported by NASA-SCAP. The authors would like to thank Parul Agrawal for her help in planning of IHF 345 and IHF 352 test series and Keith Peterson for his help in running IHF 352 tests, and the TSF test engineers involved in these tests, Frank Hui, Enrique Carballo, and Imelda Terrazas-Salinas. The support from the NASA Ames Entry Systems and Technology Division, through contract NNA15BB15C to AMA, Inc., is gratefully acknowledged.

References

- [1] Terrazas-Salinas, I., and the staff of Thermophysics Facilities Branch, "Test Planning Guide for NASA Ames Research Center Arc-Jet Complex and Range Complex," A029-9701-XM3 Rev. D, Entry Systems and Technology Division, NASA Ames Research Center, January 2018.
- [2] Gökçen, T., Skokova, K., Balboni, J. A., Terrazas-Salinas, I., and Bose, D., "Computational Analysis of Arc-Jet Wedge Calibration Tests in IHF 6-Inch Conical Nozzle," AIAA Paper 2009-1348, Jan. 2009.
- [3] Gökçen, T., Balboni, J. A., and Alunni, A. I., "Computational Simulations of the 10-MW TP3 Arc-Jet Facility," AIAA Paper 2015-3103, June 2015.
- [4] Gökçen, T., and Skokova, K. A., "CFD Simulations of the IHF Arc-Jet Flow: Compression-Pad/Separation Bolt Wedge Tests," AIAA Paper 2017-4451, June 2017.
- [5] Gökçen, T., and Alunni, A. I., "CFD Simulations of the IHF Arc-Jet Flow: 9-Inch Nozzle, Flow Surveys, LEAF Wedge Calibration Data," AIAA Paper 2019-3008, June 2019.
- [6] Fretter, E., "Interaction Heating Facility (IHF) Fact Sheet," http://www.nasa.gov/centers/ames/thermophysics-facilities-home, Thermophysics Facilities Branch, Entry Systems and Technology Division, NASA Ames Research Center, Sept. 2016.
- [7] ASTM E457-96, "Standard Test Method for Measuring Heat-Transfer Rate Using a Thermal Capacitance (Slug) Calorimeter," American Society for Testing and Materials, Ocober 1996 (Reapproved 2002, originally published in 1972).
- [8] ASTM E511-07, "Standard Test Method for Measuring Heat Flux Using a Copper-Constantan Circular Foil Heat-Flux Gage," American Society for Testing and Materials, December 2007 (original standard published in 1973).
- [9] Winovich, W., "On the Equilibrium Sonic-Flow Method for Evaluating Electric-Arc Air-Heater Performance," NASA TN-D-2132, March 1964.

- [10] Wright, M. J., Candler, G. V., and Bose, D., "Data-Parallel Line Relaxation Method for the Navier-Stokes Equations," *AIAA Journal*, Vol. 36, No. 9, 1998, pp. 1603-1609.
 - [11] Wright, M. J., "Data-Parallel Line Relaxation Code, DPLR Version 4.02," Private Communication, June 2010.
 - [12] Park, C., Nonequilibrium Hypersonic Aerothermodynamics, John Wiley & Sons, Inc., New York, 1990, Chap. 4.
- [13] Gökçen, T., Chen, Y. K., Skokova, K. A., and Milos, F. S., "Computational Analysis of Arc-Jet Stagnation Tests Including Ablation and Shape Change," *Journal of Thermophysics and Heat Transfer*, Vol. 24, No. 4, 2010, pp. 694-707; also AIAA Paper 2009-3596, June 2009.
- [14] Gökçen, T., "Effects of Test Box Pressure on Arc-Jet Flowfields and Implications for Testing," AIAA Paper 2018-3771, June 2018.
- [15] ASTM E637-05, "Standard Test Method for Calculation of Stagnation Enthalpy from Heat Transfer Theory and Experimental Measurements of Stagnation-Point Heat Transfer and Pressure," American Society for Testing and Materials, November 2005 (originally published in 1978).